Hindawi
Adsorption Science & Technology
Volume 2022, Article ID 3838766, 9 pages
https://doi.org/10.1155/2022/3838766

Research Article

Study on the Behaviors and Mechanism of Ni(II) Adsorption at the Hydroxyapatite-Water Interface: Effect of Particle Size

Xiaolan Zhao,[1,2] Wangsuo Wu,[1,2] Duoqiang Pan,[1,2] and Hanyu Wu[2,3]

[1]*Radiochemistry Laboratory, School of Nuclear Science and Technology, Lanzhou University, Lanzhou 730000, China*
[2]*Key Laboratory of Special Functional Materials and Structural Design, Ministry of Education, Lanzhou University, Lanzhou 730000, China*
[3]*Sino-French Institute of Nuclear Engineering and Technology, Sun Yat-Sen University, Zhuhai 519082, China*

Correspondence should be addressed to Hanyu Wu; wuhy76@mail.sysu.edu.cn

Received 28 July 2022; Revised 25 August 2022; Accepted 27 August 2022; Published 29 September 2022

Academic Editor: Huihui Du

Hydroxyapatite (HAP) was a highly efficient decontamination material for its strong adsorption capacity used in the immobilization of heavy metals, while the particle-size effect was insufficiently investigated during the sorption process. In the present study, the mechanisms of nickel (Ni(II)) adsorption on HAPs with two different particle sizes were investigated by combing batch experiments, desorption, and XRD analysis. The results showed that the adsorption capacity of 20 nm HAP (nano-HAP) was much higher than that of 12 μm HAP (micro-HAP). It was noticed that the results of the present study also clarified the distinct mechanisms in each adsorption process. As for micro-HAP, Ni^{2+} adsorbed through slow diffusion and replacement with Ca^{2+} and then incorporated in the lattice at pH between 6.5 and 9.0, which was confirmed by the results of kinetics, thermodynamics, and desorption. And a more compact crystalline structure and irreversible desorption behavior of micro-HAP after Ni(II) adsorption was confirmed by results of XRD and desorption isotherms, respectively. At pH > 9.0, lattice incorporation and precipitation controlled together. However, for nano-HAP, the sharp increase of Ni(II) adsorption and ionic strength dependent at pH 6.5 to 9.0 revealed that the dominant mechanisms were ionic exchange and inner-sphere complexation. XRD results showed that characteristic peaks of cassidyite appeared in Ni(II)-loading nano-HAP. At pH > 9.0, a precipitate of Ni(II) was the dominant mechanism. The experimental finds demonstrated that nanoscale HAP was a more fast, efficient, and desorbable adsorbent than micro-HAP for Ni(II) removal. These findings would be favorable for investigating the removal mechanisms of heavy metals on the HAP materials and designing the synthesis methods.

1. Introduction

Increasing human activities including mining and smelting production have resulted in growing heavy metal pollution (e.g., cadmium (Cd), lead (Pb), nickel (Ni), etc.) into the soil, water, and air [1–3]. Therefore, a fast and effective technology is urgent and important to deal with such heavy metal pollution in the environment [4–6]. Adsorption has been recognized as a clean and remarkably effective treatment technology as compared to conventional chemical precipitation, oxidation, and electrochemical [7, 8]. Common natural adsorbents studied in former research include clay minerals [9, 10], iron-manganese oxide [11, 12], and hydroxyapatite (HAP) [2, 4, 5, 8, 13–20]. Among these, HAP has gained extensive attention because of its low cost, widespread, and great adsorption capacities [21–26].

HAP is the most abundant phosphate mineral in the geological environment. Natural HAP minerals contain mainly calcium and phosphorus ($Ca_{10}(PO_4)_6(OH)_2$) [2, 27]. In addition, HAP is a kind of green and environment-friendly material, which possesses a robust hexagonal atomic framework based on two distinct calcium sites (Ca(I), Ca(II)), a tetrahedral-phosphate site, and an anion column along four edges of the unit cell [24]. Indeed, HAP turned out to be very efficient in immobilizing heavy metals in the environment, especially for Cd(II), and Pb(II) [4–6, 24, 27]. So far, dissolution-precipitation, cation exchange, and surface complexation have been proved to be the significant

mechanisms of heavy metals immobilization by HAP [2, 6]. In the dissolution-precipitation mechanism, HAP occurs a dissolution and supplies the media with phosphate ions which are capable of precipitating other surrounding metal cations (M), especially for Pb(II) [24]. This process can be portrayed by these two equations [2, 28]:

$$Ca_{10}(PO_4)_6(OH)_2 + 14\,H^+ \longrightarrow 10\,Ca^{2+} + 6\,H_2PO_4^- + 2\,H_2O, \quad (1)$$

$$10\,M^{2+} + 6\,H_2PO_4^- + 2\,H_2O \longrightarrow M_{10}(PO_4)_6(OH)_2 + 14\,H^+. \quad (2)$$

A different but equally common adsorption mechanism is cation exchange, in which metal cations could substitute the Ca sites into the HAP crystal lattice. The process was portrayed as followed [2, 28]:

$$Ca_{10}(PO_4)_6(OH)_2 + x\,M^{2+} \longrightarrow Ca_{10-x}M_x(PO_4)_6(OH)_2 + x\,Ca^{2+}. \quad (3)$$

When it comes to some metal ions such as Cd [4, 6, 14, 26, 27], Zn [14, 20], or Ni [18, 29], the cation exchange mechanism is rapid and more favorable to take place than a dissolution-precipitation process because the ionic radii of these metals are similar or smaller than Ca^{2+}(0.099 nm) [2, 6]. Moreover, according to the former studies, Ca deficiency promotes the adsorption of heavy metals on HAP [27]. Thereinto, a series of studies have confirmed Ca/P molar ratio of HAP acted as a key factor in the adsorption mechanisms [19, 20, 23, 27, 29]. Abound Ca-deficient sites and higher specific promote the heavy metals removal performance [27]. The effect of particle size on the removal of heavy metals pollution by HAP has also been studied by previous studies [30–32]. Wang et al. [31] used three particle-sized HAP to immobilize Pb in low-acidity soil and observed that HAP in the particle size of 20.08 nm has the best efficiency compared with other sizes . However, despite numerous investigations into the effect of HAP particle size, more attention has been focused on the nanoscale thus neglecting micron-scale HAP and the comparison.

Ni(II) is one of the most typical and widespread heavy metals in the environment [9, 10, 33]. A large number of previous studies investigated the adsorption mechanisms of Ni(II) on clay minerals and iron-manganese oxides [9, 10, 33]. The Ni(II) adsorption was strongly influenced by environmental factors such as pH, ionic strength, temperature, and organic matters. The primary mechanisms include ion exchange, outer-sphere complexes, inner-sphere complexes, and surface precipitates [9, 10, 33]. However, only a few studies have paid attention to the adsorption of Ni(II) on HAP [18, 34]. Mobasherpour et al., [34] revealed that the removal capacity of Pb^{2+}, Cd^{2+}, and Ni^{2+} increased in the following order: $Pb^{2+} > Cd^{2+} > Ni^{2+}$ because of the different acidity strength and ionic radii among these ions. However, the detailed mechanism of Ni(II) adsorption on HAP is not explored. Therefore, two different particle sizes of HAP were chosen to conduct the adsorption experiments with Ni(II). The aims of this study were (i) to characterize the different properties between these two types of HAP, (ii) to investigate the adsorption of Ni(II) on the HAP, and (iii) to elucidate the mechanisms of the adsorption of these two processes. The results of this study will provide important insights into the treatment of Ni(II) in the environment by using HAP.

2. Materials and Methods

2.1. Materials. All chemicals used in the experiments were purchased at analytic purity and used directly without any further purification. Hydroxyapatite (HAP) samples of 12 μm and 20 nm were purchased from Nanjing Emperor Nano Materials Co., Ltd., which were defined as micro-HAP and nano-HAP, respectively. Ni(II) stock solution (500.0 mg/L) was prepared by $Ni(NO_3)_2{\cdot}6H_2O$. All the stock solutions and suspensions were prepared with ultrapure water (18.2 MΩ·cm).

2.2. Adsorption and Desorption Experiments. The investigations of the Ni(II) behaviors and mechanisms on HAP of 12 μm and 20 nm were conducted through batch experiments in a series of 10 mL polyethylene centrifuge tubes. Certain volumes of HAP suspensions, stock solutions of $NaClO_4$ background electrolyte and Ni(II), and ultrapure water were pipetted into tubes achieving total volumes of 6.0 mL. In each adsorption system, the solid-to-liquid ratio (s/l) was maintained at 0.6 g/L, and the pH was adjusted to the desired value using a negligible volume of $HClO_4$ or NaOH solution. The pH values ranged from 4 to 11. The kinetic and thermodynamic experiments were maintained at pH 6.7 ± 0.1. Adsorption isotherms were conducted with initial concentrations from 0.8 to 66.7 mg/L. After shaking for 24 hours (kinetic experiments carried out until 72 hours) in a constant-temperature shaker (IS-RDD3, CRYSTAL) at 298 ± 1 K (thermodynamic experiments carried out at 318 ± 1 K as well), solid and liquid phases were separated by centrifugation at 12000 rpm for 30 min. The supernatant was used to determine the aqueous concentration of Ni(II) (C_e, mg/L) by spectrophotometry at a wavelength of 530 nm using dimethylglyoxime and disodium ethylenediaminetetraacetic acid. Blank samples are inserted in each batch of sample testing to control the standard deviations. The detection limit of spectrophotometry was 0.01 mg/L. The calculations of adsorption percentage (adsorption%) and adsorption quantity (Q, mg/g) of Ni(II) were illustrated in previous works [9, 35]. The solid phases were freeze-dried for further characterization. Desorption experiments were conducted following adsorption isotherms. After centrifugation, half of the supernatant was replaced by an equal volume of $NaClO_4$ background solution of pH 6.7 ± 0.1. Subsequently, the desorption systems were shaken for 168 hours at 298/318 ± 1 K and then analyzed as described in the adsorption experiments. All of the experimental data were the averages of duplicate/triplicate results, and the relative errors of data were less than 5%.

Kinetic and thermodynamic fit employed several validated models, such as pseudo-second-order, Weber-Morris, and Langmuir models, and described in detail in previous works [36, 37]. Thus, the equations and parameters would not repeat and mainly displayed key information.

2.3. Characterization. The pristine and Ni(II)-loading HAP samples were characterized in terms of morphology, specific surface area, and structure. The morphology images were obtained from a Hitachi S-4800 cold field emission high-resolution scanning electron microscope (FE-SEM). The Brunauer-Emmett-Teller (BET) method was used to determine the specific surface area of micro-HAP and nano-HAP. Brunauer-Emmett-Teller (BET) specific surface area (SSA) was measured using a Micrometrics ASAP 2020 Accelerated Surface Area. X-ray diffraction (XRD) patterns were obtained using a powder X-ray diffractometer (X' Pert PRO, Malvern PANalytical) equipped with a rotation anode using Cu-Kα radiation and operated at 40 kV and 30 mA. The scanning angle started from 5° to 65° with a step interval of 0.02° at a rate of 4.0°/min. The experimental curves were normalized to the absolute values without any smooth process and then identified the diffractions in contrast to the PDF standards of hydroxyapatite (PDF#09-0432), cassidyite (PDF#20-0228), gaspeite (PDF#12-0771), and theophrastite (PDF#14-0117) using Jade 5.0. HAP samples were measured using Nicolet Nexus 670 Fourier transform infrared spectrometer (FTIR) in the spectral range from 4000 to 400 cm^{-1}. The samples are diluted to 1% with KBr (spectrum pure). Then, the mixture was blended for 3 min and pressed to a pellet with a thickness of 10 mm at 120 Pa.

3. Results and Discussion

3.1. Characterization of HAP. HAP samples used in this study were divided into two different particle sizes including 12 μm and 20 nm, respectively. The SEM images are shown in Figure 1, and it can be noticed that micro-HAP represents an aggregative and agglomerative with a uniform spherical particle, and the surface was clean and smooth (Figure 1(a)), which exhibited a specific surface area of approximately 11.94 m^2/g. In comparison with micro-HAP, nano-HAP exhibited an amorphous feature of around 20 nm in size (Figure 1(b)). And it has been confirmed from the high specific surface area of nano-HAP about 63.53 m^2/g, which was about 5.3 times greater than that of micro-HAP. It suggested that nano-HAP possibly possessed a higher adsorption capacity to metal cations as an example of Ni(II).

The FTIR spectra of micro-HAP and nano-HAP were shown in Figure 2(a). In the range 400 to 4000 cm^{-1}, the absorption band at 3400 and 1600 cm^{-1} is mainly assigned to the OH stretching and bending vibrations of absorbed water, respectively. The hydroxyl group of hydroxyapatites exhibited characteristic spike absorption peaks at 3420 cm^{-1} and 633 cm^{-1}. The characteristic bands at 1100–1040 and 600–500 cm^{-1} were assigned to phosphate and carbonate bands at 1550, 1460, 1445, 1415, and 870 cm^{-1}. The results showed that the main functional groups of both HAP samples were consistent. And the nano-HAP contained less adsorbed water. As shown in the XRD patterns of HAP samples in Figure 2(b), compared to the PDF standard hydroxyapatite (PDF#09-0432), it can be noticed that pristine micro-HAP and nano-HAP exhibited obvious characteristic peaks at 25.88°, 31.77°, 32.20°, and 32.90° corresponding {002} and {211}, {112} and {300} crystallographic facets, respectively [5, 27].

3.2. Kinetic Estimation. The kinetics of Ni(II) adsorption on micro-HAP and nano-HAP as a function of contact time was shown in Figure 3. Knowledge of kinetics is important for the elucidation of adsorption mechanisms. From the results of kinetics, one can see that both of the adsorption with micro-HAP and nano-HAP were close to equilibrium at approximately 500 mins. This equilibrium time was longer than the adsorption time of Ni(II) on clay minerals (1-4 h) [9, 10, 30], indicating a different mechanism of adsorption between HAP and clay minerals. The adsorption capacity of nano-HAP was much higher than micro-HAP, which was consistent with the results of the specific surface area. It was worth noting that the adsorption of Ni(II) on nano-HAP has almost reached equilibrium after 500 minutes of reaction, while the micro-HAP reaction was still slowly increasing. This indicated that the mechanisms of adsorption were different between the two adsorbents.

In order to better understand the adsorption behavior and mechanism of Ni(II) on HAP, two different types of kinetic models (i.e., the pseudo-second-order model and the Weber-Morris model) were employed to simulate the interaction, and the relative parameters of each model were summarized in Table 1. One noticed that the correlation coefficient of the pseudo-second-order model was much closer to the unity of both two types of HAP (micro-HAP: $R^2 = 0.9960$; nano-HAP: $R^2 = 0.9999$), suggesting that the chemistry adsorption of Ni(II) on HAP possibly be retelimited by two different affected by two variables. The Weber-Morris model revealed that during that adsorbate uptake varies were controlled by more than one mechanism since the plot was multilinear in Figure 3 [36, 37]. The initial stage was attributed to the exterior boundary layer diffusion or instantaneous adsorption of the most readily available adsorbing sites on the HAP surface [37], while the second stage can be ascribed to the interior boundary layer diffusion [36]. It was worth noticing that the second stage was clearly different for the two-particle sizes of HA, indicating different adsorption mechanisms.

3.3. Effect of pH and Ni(II) Initial Concentration. Figure 4 showed the adsorption edge of Ni(II) on micro-HAP and nano-HAP as a function of pH at different initial Ni(II) concentrations. It can be seen that the adsorption percentage of Ni(II) on nano-HAP was much higher than on micro-HAP, which was scarcely influenced by the specific surface area. In view of this, the smaller particle size resulted in a larger specific surface area and more available adsorption sites, thus the amount of Ni adsorbed increased significantly. It was noticed that the adsorption edge of Ni(II) on micro-HAP and nano-HAP was significantly different in pH ranging from 7.5 to 9.0. For micro-HAP, the adsorption began at

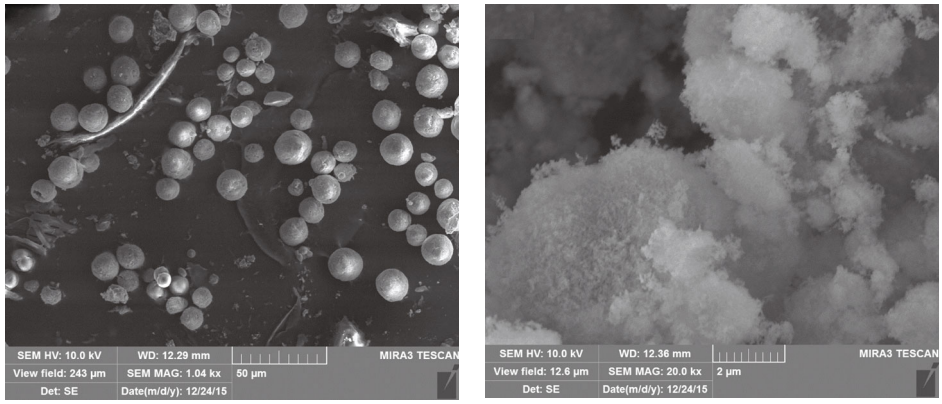

(a) (b)

Figure 1: SEM images of (a) micro-HAP (12 μm) and (b) nano-HAP (20 nm).

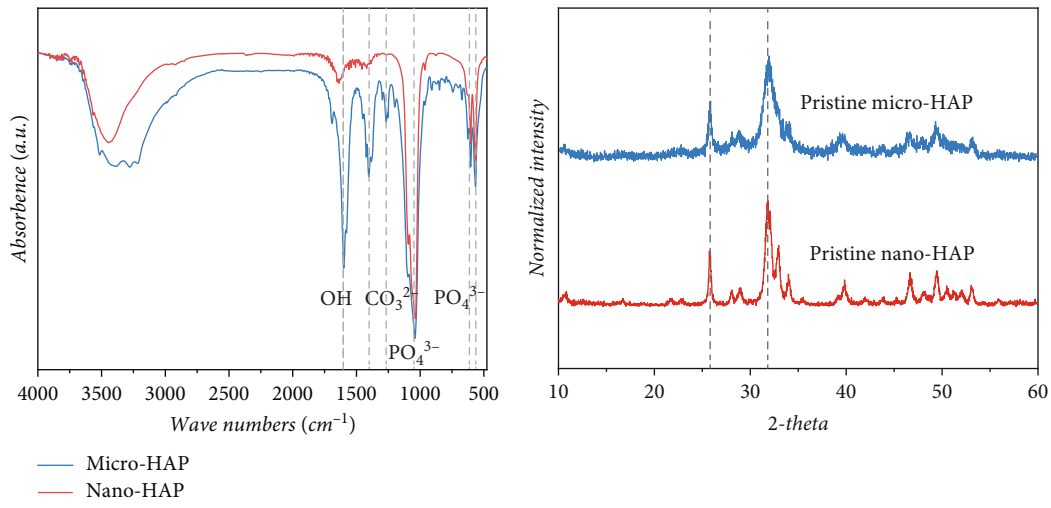

(a) (b)

Figure 2: FTIR spectrum (a) and XRD pattern (b) of micro-HAP and nano-HAP.

pH > 7.5 and with the increase of pH, the adsorption percentage exhibited steady growth. Moreover, the adsorption edge of Ni(II) on micro-HAP was independent of the initial concentration of Ni(II). Therefore, it can be assumed that at pH < 9.0, Ni(II) occurred slowly solid diffusion into the crystal lattice of micro-HAP and underwent lattice exchange with Ca(II) [2]. This pattern immobilized the Ni(II) stably. At pH > 9.0, it is controlled by both lattice exchange and precipitation mechanisms. Compared with the Ni(II) adsorption on micro-HAP, the adsorption on nano-HAP showed distinctly different mechanisms. The adsorption exhibited a start at pH > 5.0 and sparkly increased between 6.0 and 9.0. Over 90% of Ni(II) was adsorbed on nano-HAP above 9.0. The strong pH dependence suggested that the ionic exchange (IC) and inner-sphere complexes (ISCs) possibly controlled Ni(II) adsorption behavior [9]. At pH > 9.0, precipitation was the dominant mechanism. Unlike the adsorption of micro-HAP, the adsorption of Ni(II) on nano-HAP was obviously affected by the initial concentration of Ni(II). At higher initial Ni(II) concentration (50 mg/L), the adsorption shifted to higher pH with more than 1.0 pH units, which was similar to the Ni(II) uptake on illite [9].

3.4. Effect of Ionic Strength. Ionic strength is another important factor affecting the interaction, especially the adsorption behavior of heavy metals in the environment [35]. The effect of $NaClO_4$ concentration on Ni(II) adsorption by micro-HAP and nano-HAP at the pH adsorption edge was shown in Figure 5. As for micro-HAP from Figure 5(a), the adsorption of Ni(II) was completely independent of ionic strength, indicating the mechanism was without the influence of external ionic exchange. The results were mutually confirmed with the above results. Generally, the variation of ionic strength tended to affect the electrostatic interaction and outsphere surface complexes rather than lattice substitution or inner-sphere complexes [27]. In view of this, the negligible effect of ionic strength on the adsorption behavior of Ni(II) pointed the potential immobilization mechanisms of lattice replacement reaction with higher

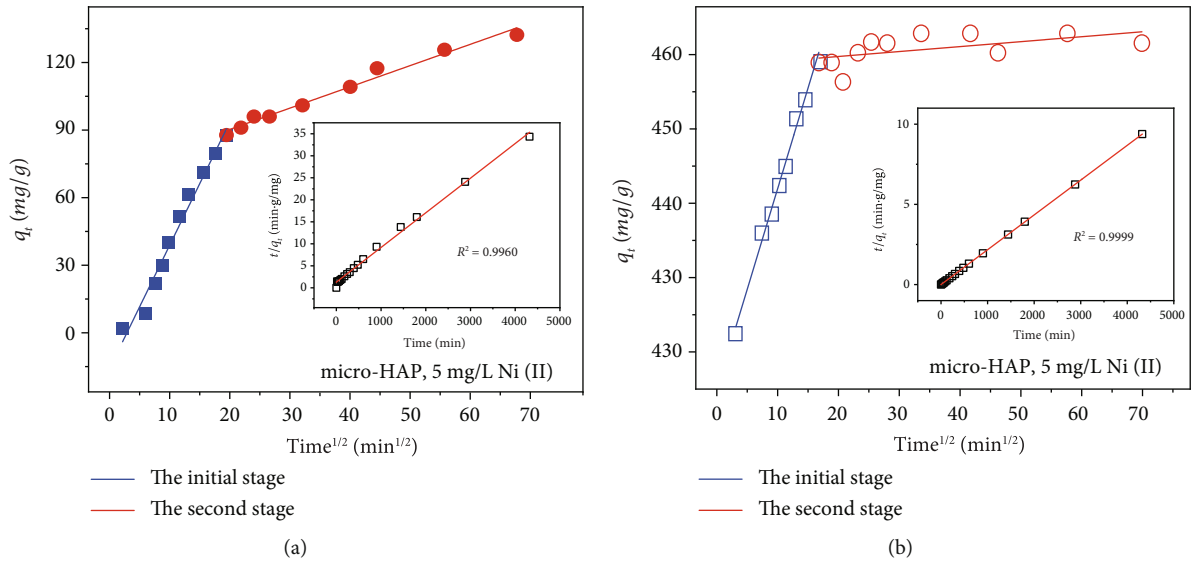

Figure 3: The kinetics of Ni(II) sorption on (a) micro-HAP and (b) nano-HAP (the solid lines: fitting plots of the Weber-Morris model). Bottom right figures: the fitting plots of the pseudo-second-order equation. ($T = 298 \pm 1\ K$, $I = 0.1$ mol/L $NaClO_4$, $s/l = 0.6$ g/L, [Ni(II)] = 5.0 mg/L, and pH = 6.7 ± 0.1).

Table 1: The parameters of pseudo-first-order and Weber-Morris models of Ni(II) adsorption on micro-HAP and nano-HAP.

Models and parameters	Micro-HAP	Nano-HAP
Pseudo-first-order model		
q_e (mg/g)	127.06	460.83
k_1 (g/mg·min)	4.75×10^{-5}	1.68×10^{-3}
R^2	0.9960	0.9999
Weber-Morris model		
$k_{id,1}$ (mg/g·min$^{-1/2}$)	5.10	2.70
C_1	-1.63	422.91
R_1^2	0.9759	0.9919
$k_{id,2}$ (mg/g·min$^{-1/2}$)	0.88	0.07
C_2	70.79	457.49
R_2^2	0.9810	0.3116

thermodynamic stability or inner-sphere complexes (i.e. the covalent binding of Ni(II) with ≡Ca-OH and ≡P-OH functional groups). In a series of former studies, the adsorption of Hg(II) and Cd(II) by HAP were also found to be the independent phenomenon of ionic strength variation [21, 27]. However, for the nano-HAP, the adsorption of Ni(II) was controlled by the ionic strength, especially between 6.5 and 8.5. There was an obvious decline in Ni(II) adsorption with the increase of the ionic strength concentrations. There may be two reasons for these phenomena. One was that ionic exchange controlled the adsorption reaction [13, 27]. Rather, higher ionic strength might cause a greater possibility for the agglomeration of nanoparticles and inhibit the adsorption of Ni(II) [27]. More characterization and experiments were needed to support the specific conclusions.

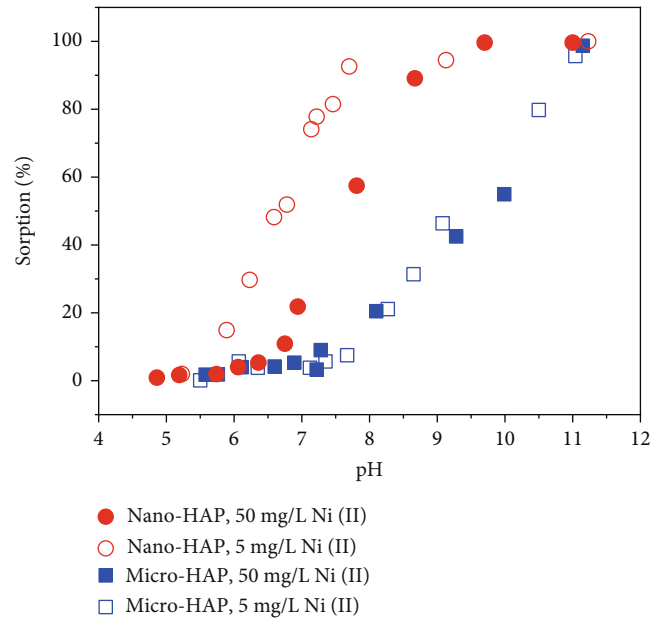

Figure 4: The influence of pH on Ni(II) sorption on micro-HAP and nano-HAP under varying nickel concentrations ($T = 298 \pm 1\ K$, $I = 0.1$ mol/L $NaClO_4$, and $s/l = 0.6$ g/L).

3.5. Thermodynamics and Desorption. Ni(II) adsorption on micro-HAP and nano-HAP with respect to the temperature effect is demonstrated in Figure 6. The solid square and circle represented adsorption isotherms at 298 and 318 K, respectively. It was obvious that the isotherms of nano-HAP were higher than micro-HAP, which was supported by adsorption % at pH 6.7 (Figure 4). The enhanced Ni(II) adsorption induced by temperature increase indicated that Ni(II) adsorption was endothermic, in accordance with the results of Ni(II) adsorption on illite [9], smectite [38], and palygorskite [10]. The temperature effect raised the rate of

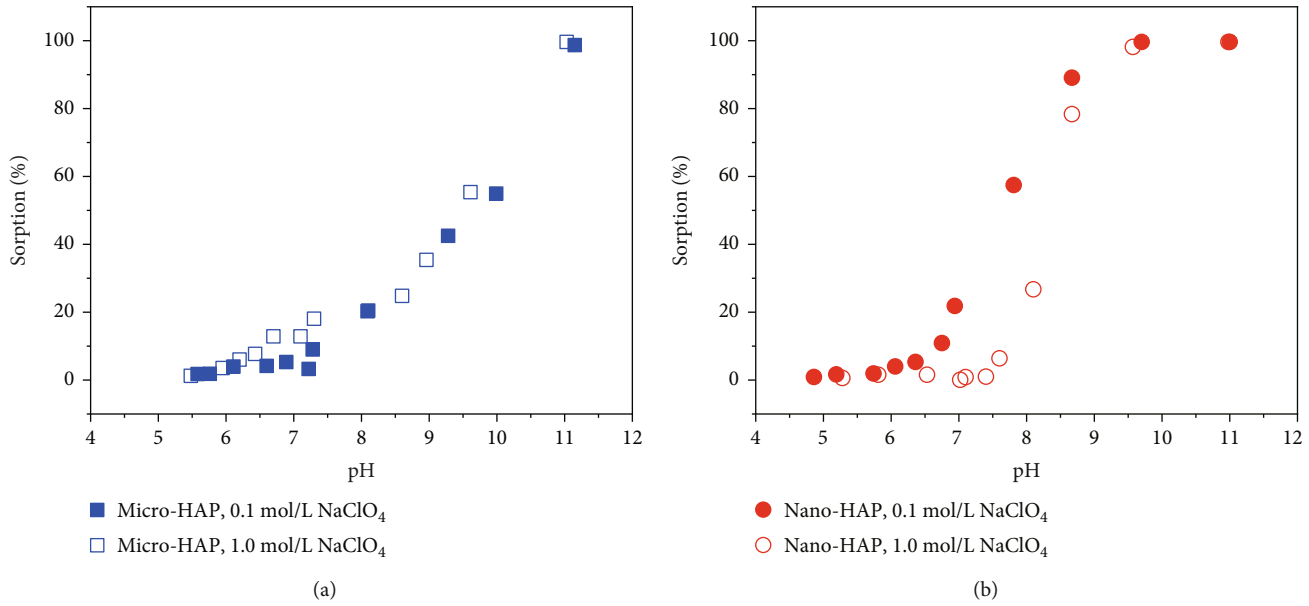

FIGURE 5: The influence of ionic strength on Ni(II) sorption on (a) micro-HAP and (b) nano-HAP ($T = 298 \pm 1\,K$, $s/l = 0.6$ g/L, and [Ni(II)] = 5.0 mg/L).

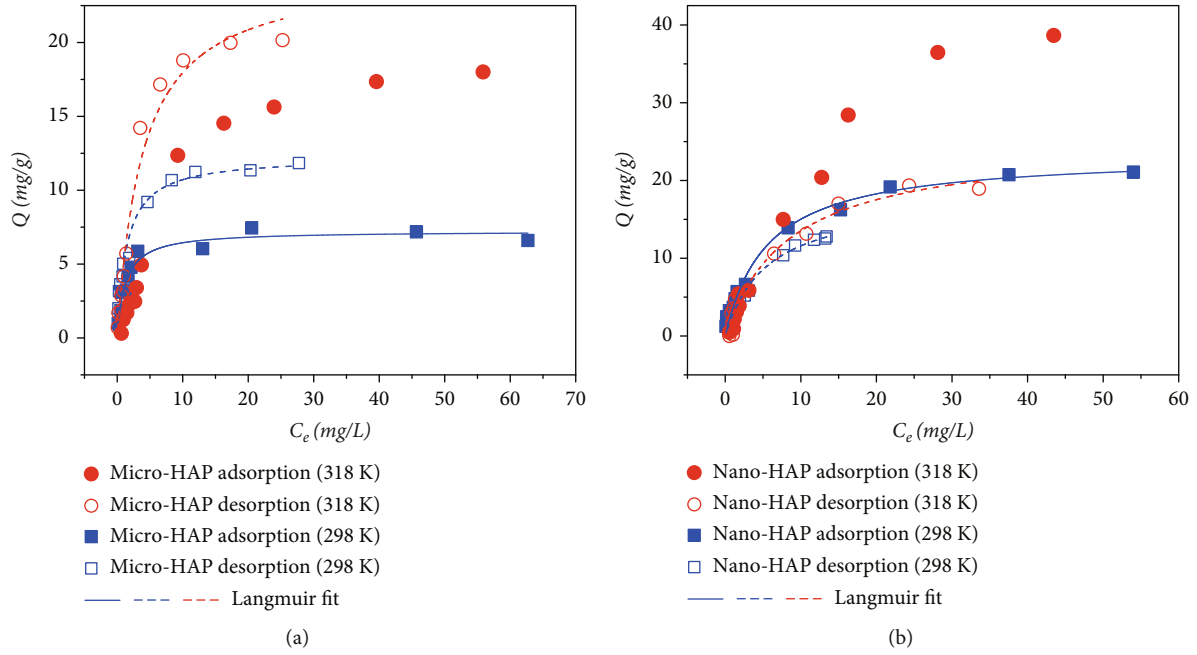

FIGURE 6: Adsorption/desorption isotherms at 298 K and 318 K of Ni(II) adsorption on (a) micro-HAP and (b) nano-HAP ($I = 0.1$ mol/L $NaClO_4$, $s/l = 0.6$ g/L, and pH = 6.7 ± 0.1).

approaching equilibrium [9, 36]. Moreover, the Langmuir fits evidenced that monolayer adsorption of Ni(II) occurred on both micro-HAP and nano-HAP even in the desorption process (Figure 6), except for the adsorption at 318 K (fitted by Freundlich model, data not shown). The parameters of Langmuir models are listed in Table 2, q_{max} supported the temperature effect on Ni(II) adsorption. Although temperature increase might cause changes in adsorption mechanism, such as accelerated adsorption at the surface of micro-HAP and nano-HAP, the monolayer adsorption equilibrium of Ni(II) reached afresh during the 168-hour desorption.

The results of desorption showed opposite phenomena in Ni(II) desorption from micro-HAP and nano-HAP (hollow square and circle). The higher desorption plots of micro-HAP represented that Ni(II) adsorption was irreversible and enlarged slowly at either 298 K or 318 K, which was verified by the kinetics of Ni(II) adsorbed on micro-HAP (Figure 6(a)). On the contrary, Ni(II) adsorption of nano-HAP was

Table 2: The Langmuir parameters of Ni(II) sorption/desorption and sorption-desorption hysteresis (HC%) on micro-HAP and nano-HAP.

Adsorption/desorption system	Langmuir model			HC%
	q_{max} (mg/g)	K_L (mL/g)	R^2	
Micro-HAP, 298 K				60.6
Adsorption	7.23	815.46	0.9480	
Desorption	12.25	695.90	0.9728	
Micro-HAP, 318 K				75.7
Adsorption	—	—	—	
Desorption	24.88	259.34	0.9736	
Nano-HAP, 298 K				-71.6
Adsorption	23.36	180.05	0.9883	
Desorption	17.94	182.66	0.9755	
Nano-HAP, 318 K				-2.0
Adsorption	—	—	—	
Desorption	24.90	118.94	0.9718	

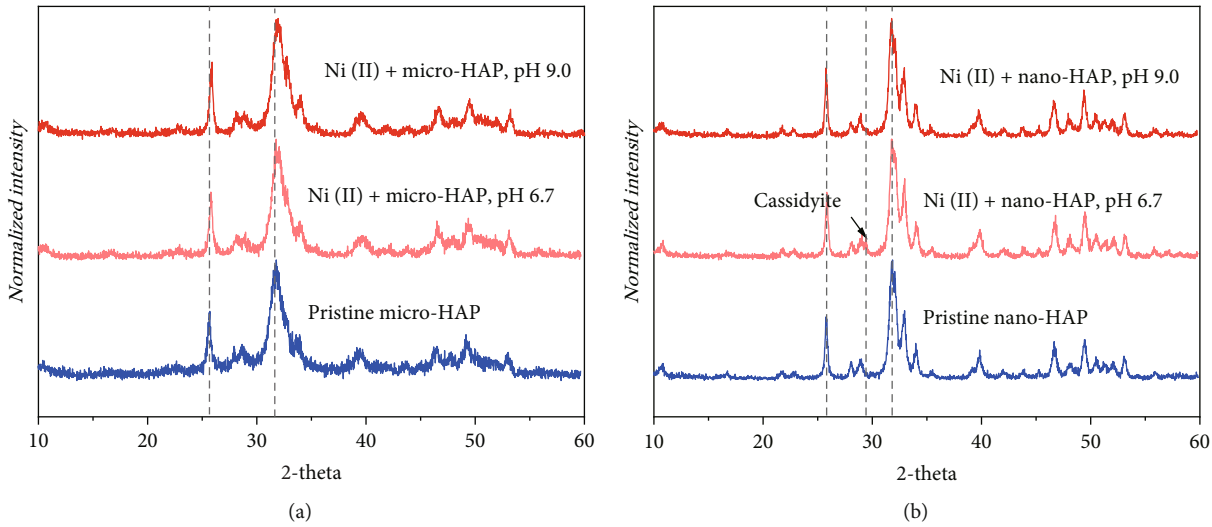

Figure 7: XRD patterns of pristine HAPs and Ni(II)-loading HAPs at pH 6.7 and 9.0. (a) micro-HAP and (b) nano-HAP.

reversible, which demonstrated that the quick ionic exchange of Ni(II) (Figure 6(b)) existed a weak bind on nano-HAP. The extents of irreversible or reversible adsorption could be quantified by the hysteresis coefficient (HC%) in Table 2, and the equation was described in previous works [36, 37].

3.6. XRD Results. XRD technique was the most intuitive and efficient method to investigate the crystal structure of materials. By comparing the crystal structures before and after adsorption experiments, it was possible to distinguish and identify the difference and mechanisms of Ni(II) on the micro-HAP and nano-HAP. The XRD patterns of pristine HAPs and adsorbed samples were shown in Figure 7. As shown in Figure 7(a), the diffraction peaks ascribed to {002} and {211} of Ni(II)-loading micro-HAP samples slightly shift towards high angles, including samples at pH 6.7 and 9.0. This phenomenon pointed to the appearance of a lattice incorporation mechanism [27]. In micro-HAP lattice, Ni^{2+} (0.072 nm) with a smaller ionic radius than Ca^{2+} (0.099 nm) substituted Ca^{2+}. The lattice replacement implied the enhancement of the entire micro-HAP crystalline structure and verified the effectiveness of Ni(II) substitution. Thus, it can be seen that the crystallization and orientation were enhanced by Ni(II) adsorption. These results also verified the previously speculated mechanism of *Ni(II)* adsorption on micro-HAP, in which Ni was slowly diffused into the HAP lattice and underwent lattice substitution with Ca^{2+}. This adsorption form and mechanism was stable and irreversible. Compared with the XRD patterns of Ni(II) adsorption on micro-HAP, there was no obvious shift in XRD patterns of Ni(II) adsorption on nano-HAP. However, there was a small peak at approximately 29° of the XRD pattern of nano-HAP adsorption sample at pH 6.7. Based on the comparison, this band might be

associated with the characteristic peak of the cassidyite ($Ca_2Ni(PO_4)_2{\cdot}2H_2O$), indicating that Ni(II) underwent ionic exchange with Ca^{2+}. There was neither a shift nor a new peak in XRD pattern of Ni(II) adsorption on nano-HAP at pH 9.0, indicating that precipitation of Ni(II) was the dominant mechanism at pH 9.0. It was consistent with the results of the ionic strength effect.

4. Conclusion

This work integrally investigated the different mechanisms of Ni(II) adsorption on HAP with two different particle sizes (12 μm and 20 nm). These two different HAPs exhibited specific surface areas and crystal structures, resulting in significant differences in the behaviors and mechanisms of Ni(II) adsorption. The results showed that adsorption percentage of Ni(II) on nano-HAP was much higher than that on micro-HAP, and it was inhibited by initial Ni(II) concentration and ionic strength only in the nano-HAP adsorption systems at pH 6.5-9.0. Nevertheless, Ni(II) adsorption on micro-HAP was independent of both Ni(II) concentration and ionic strength. These results implied the effect of particle size of HAPs, which was further investigated in adsorption/desorption isotherms at 298 K and 318 K. It can be summarized that the adsorption of Ni(II) on micro-HAP was mainly controlled by the slow diffusion and incorporation with Ca^{2+} from pH 6.5-9.0. At pH > 9.0, precipitation mechanisms are incorporated, but lattice incorporation still played a dominant role. The adsorption of Ni(II) on micro-HAP was spontaneous, endothermic, and irreversible. As for nano-HAP, a sharp increase in adsorption of Ni(II) from pH 6.5 to 9.0 mainly revealed that the adsorption was controlled by the ionic exchange and ISCs. When the pH increased to 9.0, precipitation was the dominant mechanism. These findings revealed that the nanoscale HAP removed heavy metals more effectively than microscale and provided a new perspective on condition control and material structure design for using HAP to remove the heavy metals contamination in the environment.

Data Availability

All data are available on request from the authors.

Conflicts of Interest

The authors declare that they have no conflicts of interest.

Acknowledgments

This work was supported by the National Natural Science Foundation of China [grant numbers 21906187], the China Postdoctoral Science Foundation (2021 M691372), the Fundamental Research Funds for the Central Universities [grant number lzujbky-2022-kb01], and the Key Laboratory Project of Gansu Province (1309RTSA041).

References

[1] X. L. Zhao, B. H. He, H. Y. Wu et al., "A comprehensive investigation of hazardous elements contamination in mining and smelting-impacted soils and sediments," *Ecotoxicology and Environmental Safety*, vol. 192, article 110320, 2020.

[2] M. Ibrahim, M. Labaki, J. M. Giraudon, and J. F. Lamonier, "Hydroxyapatite, a multifunctional material for air, water and soil pollution control: a review," *Journal of Hazardous Materials*, vol. 383, article 121139, 2020.

[3] Y. P. Yan, B. Wan, M. Mansor et al., "Co-sorption of metal ions and inorganic anions/organic ligands on environmental minerals: a review," *Science of the Total Environment*, vol. 803, article 149918, 2022.

[4] M. M. Wu, L. M. Mo, and E. Bi, "Effects of fulvic acid and montmorillonite colloids at different concentrations on Cd(II) sorption onto nano-hydroxyapatite," *Chemosphere*, vol. 248, article 125992, 2020.

[5] C. L. Zhou, X. Y. Wang, X. Song et al., "Insights into dynamic adsorption of lead by nano-hydroxyapatite prepared with two-stage ultrasound," *Chemosphere*, vol. 253, article 126661, 2020.

[6] C. L. Zhou, X. Song, Y. W. Wang, H. Wang, and S. F. Ge, "The sorption and short-term immobilization of lead and cadmium by nano- hydroxyapatite/biochar in aqueous solution and soil," *Chemosphere*, vol. 286, Part 3, article 131810, 2022.

[7] Y. H. Zhang, C. Q. Zhu, F. Q. Liu, Y. Yuan, H. D. Wu, and A. Li, "Effects of ionic strength on removal of toxic pollutants from aqueous media with multifarious adsorbents: a review," *Science of the Total Environment*, vol. 646, pp. 265–279, 2019.

[8] A. Nayak and B. Bhushan, "Hydroxyapatite as an advanced adsorbent for removal of heavy metal ions from water: focus on its applications and limitations," *Materials Today: Proceedings*, vol. 46, pp. 11029–11034, 2021.

[9] X. L. Zhao, S. R. Qiang, H. Y. Wu et al., "Exploring the sorption mechanism of Ni(II) on illite: batch sorption, modelling, EXAFS and extraction investigations," *Scientific Reports*, vol. 7, no. 1, p. 8495, 2017.

[10] X. X. Mo, M. G. Siebecker, W. X. Gou, and W. Li, "EXAFS investigation of Ni(II) sorption at the palygorskite-solution interface: new insights into surface-induced precipitation phenomena," *Geochimica et Cosmochimica Acta*, vol. 314, pp. 85–107, 2021.

[11] D. Ociński, I. Jacukowicz-Sobala, P. Mazur, J. Raczyk, and E. Kociołek-Balawejder, "Water treatment residuals containing iron and manganese oxides for arsenic removal from water - characterization of physicochemical properties and adsorption studies," *Chemical Engineering Journal*, vol. 294, pp. 210–221, 2016.

[12] C. M. McCann, C. L. Peacock, K. A. Hudson-Edwards, T. Shrimpton, N. D. Gray, and K. L. Johnson, "In situ arsenic oxidation and sorption by a Fe-Mn binary oxide waste in soil," *Journal of Hazardous Materials*, vol. 342, pp. 724–731, 2018.

[13] Y. J. Lee, E. J. Elzinga, and R. J. Reeder, "Sorption mechanisms of zinc on hydroxyapatite: systematic uptake studies and EXAFS spectroscopy analysis," *Environmental Science & Technology*, vol. 39, no. 11, pp. 4042–4048, 2005.

[14] A. Corami, S. Mignardi, and V. Ferrini, "Cadmium removal from single- and multi-metal (Cd+Pb+Zn+Cu) solutions by sorption on hydroxyapatite," *Journal of Colloid and Interface Science*, vol. 317, no. 2, pp. 402–408, 2008.

[15] F. Fernane, M. O. Mecherri, P. Sharrock, M. Hadioui, H. Lounici, and M. Fedoroff, "Sorption of cadmium and

copper ions on natural and synthetic hydroxylapatite particles," *Materials Characterization*, vol. 59, no. 5, pp. 554–559, 2008.

[16] D. X. Liao, W. Zheng, X. M. Li et al., "Removal of lead(II) from aqueous solutions using carbonate hydroxyapatite extracted from eggshell waste," *Journal of Hazardous Materials*, vol. 177, no. 1-3, pp. 126–130, 2010.

[17] Z. Z. Zhang, M. Y. Li, W. Chen, S. Z. Zhu, N. N. Liu, and L. Y. Zhu, "Immobilization of lead and cadmium from aqueous solution and contaminated sediment using nano-hydroxyapatite," *Environmental Pollution*, vol. 158, no. 2, pp. 514–519, 2010.

[18] I. Mobasherpour, E. Salahi, and M. Pazouki, "Removal of nickel (II) from aqueous solutions by using nano-crystalline calcium hydroxyapatite," *Journal of Saudi Chemical Society*, vol. 15, no. 2, pp. 105–112, 2011.

[19] W. Q. Tang, R. Y. Zeng, Y. L. Feng, X. M. Li, and W. Zhen, "Removal of Cr(VI) from aqueous solution by nano-carbonate hydroxylapatite of different Ca/P molar ratios," *Chemical Engineering Journal*, vol. 223, pp. 340–346, 2013.

[20] K. Viipsi, S. Sjöberg, K. Tõnsuaadu, and A. Shchukarev, "Hydroxy- and fluorapatite as sorbents in Cd(II)-Zn(II) multi-component solutions in the absence/presence of EDTA," *Journal of Hazardous Materials*, vol. 252-253, pp. 91–98, 2013.

[21] Y. Kim and Y. J. Lee, "Characterization of mercury sorption on hydroxylapatite: batch studies and microscopic evidence for adsorption," *Journal of Colloid and Interface Science*, vol. 430, pp. 193–199, 2014.

[22] A. A. Rouff, N. Ma, and A. B. Kustka, "Adsorption of arsenic with struvite and hydroxylapatite in phosphate-bearing solutions," *Chemosphere*, vol. 146, pp. 574–581, 2016.

[23] S. Campisi, C. Castellano, and A. Gervasini, "Tailoring the structural and morphological properties of hydroxyapatite materials to enhance the capture efficiency towards copper(II) and lead(II) ions," *New Journal of Chemistry*, vol. 42, no. 6, pp. 4520–4530, 2018.

[24] D. X. Guan, C. Ren, J. Wang, Y. Zhu, Z. Zhu, and W. Li, "Characterization of lead uptake by nano-sized hydroxyapatite: a molecular scale perspective," *ACS Earth and Space Chemistry*, vol. 2, no. 6, pp. 599–607, 2018.

[25] M. Ferri, S. Campisi, M. Scavini, C. Evangelisti, P. Carniti, and A. Gervasini, "In-depth study of the mechanism of heavy metal trapping on the surface of hydroxyapatite," *Applied Surface Science*, vol. 475, pp. 397–409, 2019.

[26] X. Han, Y. Zhang, L. Y. Li et al., "Nanosized hydroxyapatite supported on natural sepiolite: a novel adsorbent for cd(II) removal from simulated groundwater," *Materials Research Express*, vol. 6, no. 12, article 125518, 2019.

[27] Y. W. Zhang, H. Y. Tang, Q. Xiao, Y. Zhang, X. L. Zhao, and S. T. Yang, "New strumming sleight for old tunes: exploration on the sorption mechanisms of Cd(II) by hydroxyapatite synthesized with different molar Ca/P ratios," *Journal of Environmental Chemical Engineering*, vol. 10, no. 3, article 107919, 2022.

[28] C. Stötzel, F. A. Müller, F. Reinert, F. Niederdraenk, J. E. Barralet, and U. Gbureck, "Ion adsorption behaviour of hydroxyapatite with different crystallinities," *Colloids and Surfaces B: Biointerfaces*, vol. 74, no. 1, pp. 91–95, 2009.

[29] S. Rout, N. Khandelwal, A. K. Poswal, V. Pulhani, and A. V. Kumar, "Inducing non-stoichiometry in nano-hydroxyapatite for ultra-fast sequestration of uranyl ions in water: mechanism delineation using XAS," *Environmental Science Nano*, vol. 8, no. 5, pp. 1256–1268, 2021.

[30] W. Liu, G. M. Qian, L. L. Liu, B. Zhang, and X. Y. Fan, "A simple method to controlled synthesis of nano hydroxyapatite in different particle size," *Materials Letters*, vol. 217, pp. 177–180, 2018.

[31] Y. Wang, X. Q. Dong, J. Cui, Z. G. Wei, and X. H. Wang, "Effect of hydroxyapatite particle size on the formation of chloropyromorphite in anglesite–hydroxyapatite suspensions," *RSC Advances*, vol. 7, no. 20, pp. 11896–11903, 2017.

[32] Z. Zhao, G. Jiang, and R. Mao, "Effects of particle sizes of rock phosphate on immobilizing heavy metals in lead zinc mine soils," *Journal of Soil Science and Plant Nutrition*, vol. 14, 2014.

[33] B. Gueguen, J. V. Sorensen, S. V. Lalode, J. Pena, B. M. Toner, and O. Rouxel, "Variable Ni isotope fractionation between Fe-oxyhydroxides and implications for the use of Ni isotopes as geochemical tracers," *Chemical Geology*, vol. 481, pp. 38–52, 2018.

[34] I. Mobasherpour, E. Salahi, and M. Pazouki, "Comparative of the removal of Pb^{2+}, Cd^{2+} and Ni^{2+} by nano crystallite hydroxyapatite from aqueous solutions: adsorption isotherm study," *Arabian Journal of Chemistry*, vol. 5, no. 4, pp. 439–446, 2012.

[35] X. L. Zhao, Y. Wang, H. Y. Wu et al., "Insights into the effect of humic acid on Ni(II) sorption mechanism on illite: batch, XPS and EXAFS investigations," *Journal of the Molecular Liquids*, vol. 248, pp. 1030–1038, 2017.

[36] H. Y. Wu, P. Li, D. Q. Pan, Z. X. Yin, Q. H. Fan, and W. S. Wu, "Interactions between silicon oxide nanoparticles (SONPs) and U(VI) contaminations: effects of pH, temperature and natural organic matters," *PLoS One*, vol. 11, article 0149632, 2016.

[37] H. Y. Wu, Z. Xu, L. Zhu, X. Cheng, and M. L. Kang, "Adsorption of strontium at K-feldspar-water interface," *Applied Radiation and Isotopes*, vol. 181, article 110111, 2022.

[38] E. Tertre, G. Berger, S. Castet, M. Loubet, and E. Giffaut, "Experimental sorption of Ni^{2+}, Cs^{+} and Ln^{3+} onto a montmorillonite up to 150°C," *Geochimica et Cosmochimica Acta*, vol. 69, no. 21, pp. 4937–4948, 2005.